HHS Public Access

Author manuscript

Mol Pharm. Author manuscript; available in PMC 2019 December 28.

Published in final edited form as:

Mol Pharm. 2019 March 04; 16(3): 1412–1420. doi:10.1021/acs.molpharmaceut.8b01278.

Linear Desferrichrome-Linked Silicon–Rhodamine Antibody Conjugate Enables Targeted Multimodal Imaging of HER2 in Vitro and in Vivo

Shin Hye Ahn, **Daniel Thach**, **Brett A. Vaughn**, **Vincent M. Alford**, **Alyssa N. Preston**, **Scott T. Laughlin**, **Eszter Boros***

Department of Chemistry, Stony Brook University, 100 Nicolls Road, Stony Brook, New York 11790, United States

Abstract

We report the nuclear and optical in vitro and in vivo imaging of SKOV-3 cells by targeting HER2 with a bimodal trastuzumab conjugate. Previously, we have shown that desferrichrome derivatives provide a robust and versatile radiolabeling platform for the radioisotope zirconium-89. Here, we appended silicon-rhodamine functionalized linear desferrichrome to trastuzumab. This construct was radiolabeled and used to image cellular binding and antibody uptake in vitro and in vivo. The robust extinction coefficient of the SiR deep-red emissive fluorophore enables direct quantification of the number of appended chelators and fluorophore molecules per antibody. Subsequent radiolabeling of the multifunctional immunoconjugate with ^{89}Zr was achieved with a 64 ± 9% radiochemical yield, while the reference immunoconjugate desferrioxamine (DFO)-trastuzumab exhibited a yield of 84 ± 9%. In vivo PET imaging (24, 48, 72, and 96 h post injection) and biodistribution experiments (96 h post injection) in HER2+ tumor bearing mice revealed no statistically significant difference of the two ^{89}Zr-labeled conjugates at each time point evaluated. The bimodal conjugate permitted successful in vivo fluorescence imaging (96 h post injection) and subsequent fluorescence-guided, surgical resection of the tumor mass. This report details the first successful application of a fluorophore-functionalized desferrichrome derivative for targeted imaging, motivating further development and application of this scaffold as a multimodal imaging platform.

Graphical Abstract

***Corresponding Author:** eszter.boros@stonybrook.edu; Phone: +1 (631) 632-8572; Fax: +1 (631) 632-7960.

The authors declare no competing financial interest.

Supporting Information

The Supporting Information is available free of charge on the ACS Publications website at DOI: 10.1021/acs.molpharmaceut.8b01278. UV–vis absorbance values, LC–UV–TOF mass spectra, method for quantification of the fluorophore–antibody ratio, immunoreactivity data, ROI analyses of PET/CT images at all time points, and in vivo fluorescence images (PDF)

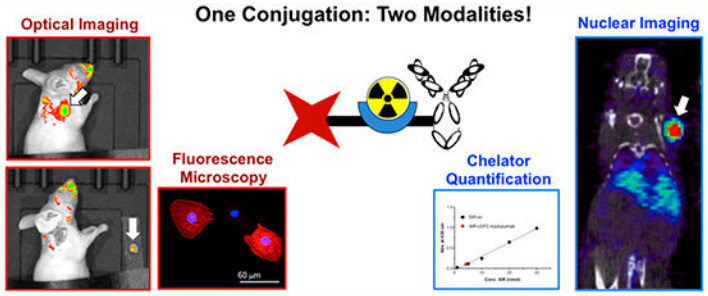

Keywords

desferrichrome; silicon–rhodamine; zirconium-89; multimodality; trastuzumab

INTRODUCTION

Targeted molecular imaging in a clinical setting provides a noninvasive approach to diagnose and localize disease with potential implications in both predicting treatment outcome in addition to monitoring patient response to therapy. The ideal targeted molecular imaging probe exhibits high target efficacy, ideal imaging pharmacokinetics, metabolic stability, and low off-target uptake; these properties can be tuned through chemical probe design and subsequent preclinical, in vitro and in vivo assessment. Currently, over 100 phase I–III clinical trials employ radiolabeled antibodies as tools to evaluate the extent of disease and predict response to immunotherapy. The zirconium-89-radiolabeled conjugate DFO-trastuzumab is currently being evaluated in various clinical trials to predict the treatment efficacy of breast cancer with the human epidermal growth factor 2 (HER2)-targeting trastuzumab or trastuzumab-emtansine.[3–5] The increasing number of new studies with radiolabeled antibody conjugates demonstrates their increasing utility and importance in research comparable to the popularity of other mainstay radiological tracers, such as ^{99m}Tc-sestamibi and ^{18}F-FDG.[6–10]

In a typical clinical setting, patient body scans are performed using targeted nuclear tracers to determine the extent of disease, which helps guide decisions on the course of treatment recommended moving forward. Upon evaluation of the tumor burden, surgical resection of an operable tumor is carried out, followed by subsequent implementation of conventional chemotherapeutic intervention strategies.[11,12] If surgery is carried out shortly after the nuclear imaging procedure, intraoperative radioguidance can be employed to indicate areas of disease in combination with classical methods of inspection of the tissue by eye and manual palpation. The disadvantage of this method is the lack of resolution and accuracy to properly delineate tumor margins.[15] Alternatively, fluorescent probes can provide clear visualization of tumor margins due to the high spatial resolution of detectable fluorescence emission. Indocyanine green, indocyanine green-folate (OTL38), and IRDye800CW (conjugated to targeting vectors, such as bombesin or panitumomab) are currently under clinical investigation as tools for fluorescence-guided surgery. In addition to guiding surgical intervention, the fluorescence label can be detected during the histological characterization

of the resected mass, thereby imparting additional information about tumor heterogeneity and cell surface cancer-associated biomarkers to the pathologists.[16,17]

The direct combination of targeted nuclear tracers and fluorescence imaging modalities has the potential to provide a single molecular probe that can be used to seamlessly carry out whole body imaging, followed by immediate fluorescence-guided surgical intervention.[12,18] Multimodality probes can be attained either through stepwise or concerted attachment of both labels to the targeting vector (Figure 1).[1,2,14] Advances have been made in radiolabeling functionalized nanoparticles for PET/NIRF or SPECT/NIRF imaging; however, accumulation of NPs in hepatobiliary organs remains a challenge.[19] For monoclonal antibodies, the stepwise attachment has been explored more extensively and more successfully, but this approach poses numerous limitations.[1,20] If both labels are introduced separately by conjugation to reactive functional groups on the antibody, reactivity of one or both components may be limited, and products can exhibit significant batch variation. Furthermore, various reports detail the correlation between an increasing number of attached fluorophores and a pronounced decline of target-to-background ratios, arising from pronounced hepatic or lung uptake.[20] Additional issues can arise due to challenges associated with accurately determining the total number of attached fluorophore and chelator of a sequentially conjugated product, such as IRDye800-trastuzumab-DTPA (Figure 2).[1] This necessitates characterization following each conjugation. For example, mass spectrometry or isotope dilution assays are used to quantify the chelators, and the antibody–fluorophore ratio is determined by comparing UV–vis absorbance of the immunoconjugate at 280 nm (corresponding to antibody absorption) and the excitation wavelength of the fluorophore.

Our group and others have worked toward chemical solutions to address these shortcomings by designing bifunctional constructs that incorporate both nuclear and optical modalities to be appended to the antibody in one single step. Josephson and co-workers reported the use of a Lys-Lys-βAla-Lys(N_3) as a scaffold for covalently attaching DOTA and CyAL5.5 fluorophore and coupling to a RGD- or RAD-targeting peptide via strain-promoted azide–alkyne cycloaddition for targeted multimodal imaging study.[21] In 2012, Hendricks et al. proposed the application of 18F-labeled BODIPY fluorophore as a bifunctional imaging probe.[13] The BODIPY fluorophore displays robust quantum yields, is stable in physiological conditions, and exhibits chemical versatility exemplified by the wide range of functionalizations reported.[22] However, despite optimized transfluorination procedures that allow for complete radiolabeling within a few minutes, [^{18}F]BODIPY is not suitable for antigen-targeted bimodal imaging for various reasons. First, the disparity between the radioisotope half-life (1.83 h) and metabolic half-life of antibodies (72–96 h) results in a low target-to-background ratio at early imaging time points commonly employed for ^{18}F. Second, the reaction conditions to introduce ^{18}F onto BODIPY are incompatible with the chemically sensitive nature of antibodies.

Previously, Meimetis and co-workers have reported the synthesis and application of a fluorogenic linker moiety to incorporate the fluorophore BODIPY with an appended desferioxamine (DFO) chelator for radiolabeling with ^{89}Zr ($t_{1/2}$ = 78 h) to the HER2-targeting antibody trastuzumab (Figure 2).[14] While the fluorescence of this probe emerges as

conjugation occurs and provides a convenient handle for reaction control, a two-step functionalization is still required; furthermore, the biodistribution profile is significantly altered in comparison with ^{89}Zr-DFO-trastuzumab, and in vivo fluorescence imaging is not possible due to the short-wave emission of the BODIPY fluorophore. Maindron and co-workers conjugated BODIPY with styryl functional groups to red shift the excitation and emission wavelengths into the therapeutic window (Figure 2).[2] In order to compensate for the high lipophilicity of 3,5-distyryl BODIPY, the fluorophore is coupled to three 1,4,7,10-tetraazacyclododecane-1,4,7,10-tetraacetic acid (DOTA) molecules and, thereafter, conjugated to trastuzumab to form tris-DOTA-BODIPY-trastuzumab. However, a significant increase of typical liver uptake arising from the appended lipophilic fluorophores is still observed. These studies showed that significant improvements to multimodal probe design were required to improve the ease of application, guarantee more uniform pharmacokinetics, and enhance applicability for in vivo imaging. The following properties were considered essential, (1) introduction of the fluorophore–chelator construct must be attainable in one step; (2) chelation of the radioisotope, followed by radiochemical complex stability to impart nuclear imaging capabilities, can not be impeded by the presence of fluorophore; (3) the pharmacokinetics of the antibody cannot be drastically altered when compared to nuclear modality-only conjugates; and (4) the emissive properties of the fluorophore must enable in vitro, intrasurgical, and in vivo (through-skin) imaging of the target.

We have already successfully demonstrated the chemical synthesis of linear desferrichromes, which provide a convenient, easily functionalizable chelator platform for radiolabeling with ^{89}Zr.[23] Here, we report the application of silicon–rhodamine (SiR)-linked linear desferrichrome (LDFC) conjugated to trastuzumab (SiR-LDFC-trastuzumab) for conjugate characterization, confocal microscopy imaging of probe internalization, in vivo PET and fluorescence imaging, as well as fluorescence-guided surgery.

EXPERIMENTAL SECTION

General Methods.

All starting materials were purchased from Acros Organics, Sigma-Aldrich, Macrocyclics, or TCI America and used without further purification.

Mass Spectrometry.—Low-resolution electrospray ionization (ESI) mass spectrometry and high-resolution ESI mass spectrometry were carried out at the Stony Brook University Institute for Chemical Biology and Drug Discovery (ICB&DD) Mass Spectrometry Facility. Mass of the immunoconjugate was determined on an Agilent LC–UV–TOF, using method A (Aeris XB-38, 3.6 μm, 300 Å, 150 × 2.1 mm; solvent A, H_2O (0.01% Ac, 0.02% TFA); solvent B, CH_3CN:2-PrOH (9:1, 0.1% Ac, 0.02% TFA); t = 0–1′, B = 10%; t = 1–31′, B = 10–95%; 0.50 mL/min; T = 60 °C).

UV–vis.—UV–vis spectra were collected with the NanoDrop ^{1}C instrument (AZY1706045). Spectra were recorded from 200 to 900 nm in a quartz cuvette with 1 cm path length.

Immunoconjugate Concentration.—Immunoconjugate concentration was determined using the NanoDrop Protein Quantification tool.

High Performance Liquid Chromatography (HPLC).—Preparative HPLC was carried out using a Shimadzu HPLC-20AR equipped with a binary gradient, pump, UV–vis detector, and manual injector on a Phenomenex Luna C18 column (250 mm × 21.2 mm, 100 Å, AXIA packed). Method B (preparative purification method): A = 0.1% TFA in water, B = 0.1% TFA in MeCN. Gradient: 0–5 min, 95% A; 5–24 min, 5–95% B.

Synthesis and Antibody Conjugation.

The synthesis of *N*-(10-(2-Carboxy-4-(((5*S*,8S,11*S*)-15-hydroxy-5,8-bis(3-(*N*-hydroxyacetamido)propyl)-11-(3-(4-isothiocyanatophenyl)-thioureido)-4,7,10,16-tetraoxo-3,6,9,15-tetraazaheptadecyl)-carbamoyl)phenyl)-7-(dimethylamino)-5,5-dimethyldibenzo-[b,e]silin-3(5H)-yli-dene)-*N*-methylmethanaminium and its conjugation to trastuzumab were performed according to a literature method (Figure 3).[23] A 100 μL solution of trastuzumab in PBS (6.4 mg/mL, 4.4 nmol) was diluted with 500 μL of 0.1 M $NaHCO_3$ (pH 9.0). Then, 3.0 mg of SiR-LDFC-Ph-NCS (2.4 μmol) was dissolved in 200 μL of DMSO, and 20 μL of this solution (0.24 μmol) was added to the trastuzumab solution. The reaction was incubated at room temperature for 18 h. DFO-trastuzumab was prepared using a 100 μL solution of trastuzumab in PBS (5.6 mg/mL, 3.9 nmol). Then, 500 μL of 0.1 M $NaHCO_3$ (pH 9.0) was added to this solution, followed by 0.1 mg of *p*-SCN-Ph-deferoxamine (13 nmol) in 20 μL of DMSO. The reaction was incubated at room temperature for 18 h. Following incubation, both immunoconjugate samples were purified using 5 mL Zeba size exclusion desalting columns and characterized via LC–UV–TOF MS. SiR-LDFC-trastuzumab was further characterized via UV–vis measurements (Table S1).

Quantification of Fluorophore on Trastuzumab.

Absorbance at 630 nm was measured for SiR-ethylenediamine (SiR-en) samples on the NanoDrop, with the concentration ranging from 1 to 50 μM. The resulting calibration curve was used to determine the SiR concentration from the absorbance of SiR-LDFC-trastuzumab at 630 nm (Figure 4, Table S1, $\varepsilon = 30794\ M^{-1}cm^{-1}$). The antibody concentration was determined using the NanoDrop Protein Quantification tool, and the ratio of SiR to trastuzumab was calculated to be 1.03, under the assumption that extinction coefficients of antibody bound and nonconjugated species are not significantly different.

SDS PAGE of SiR-LDFC-trastuzumab.

Immunoconjugate samples were prepared with 2× Laemmli Buffer and βME in a 1:1 ratio. For complete reduction, the samples (3 μg in 10 μL) were heated at 70°C for 10 min and then loaded onto a 7.5% polyacrylamide gel (TGX FastCast). Electrophoresis was performed for 45 min at 150 V. The gel was subjected to fluorescence imaging using a phosphorimager (Typhoon 9400, Amersham Biosciences) to detect fluorescent bands with an SiR label. Emission at 633 nm wavelength was used to visualize fluorescence (Figure 5). Subsequently, Coomassie staining was used to visualize ladder and protein samples within the gel.

Radiolabeling.

$^{89}Zr(oxalate)_4$ was received from the University of Wisconsin—Madison. Upon receipt, the pH was adjusted to 6.8–7.5 using 0.1 M Na_2CO_3. Then, 150 μg of SiR-LDFC-trastuzumab or DFO-trastuzumab in 300 μL of chelex-resin-treated dPBS (pH 7.4) was incubated with 9.69 MBq (261 μCi) of $^{89}Zr(oxalate)_4$ for 60 min at room temperature. The progress of radiolabeling was monitored with radio-TLC (solid phase, Sigma-Aldrich; silica gel on TLC aluminum foils, 10 × 70 mm; mobile phase, 50 mM EDTA, pH 7), and the resulting radio-immunoconjugate was purified on a 5 mL Zeba size exclusion desalting column. The isolated radiochemical yield was 64 ± 9% for ^{89}Zr-SiR-LDFC-trastuzumab and 84 ± 9% for ^{89}Zr-DFO-trastuzumab, with specific activities of 30.7 ± 6.3 and 28.5 ± 3.3 MBq/mg, respectively.

Immunoreactivity Assay.

The immunoreactivity of ^{89}Zr-SiR-LDFC-trastuzumab was determined from cellular-binding assays. SKOV-3 cells were suspended in microcentrifuge tubes at concentrations of 0.25, 0.5, 0.75, 1.0, 1.25, and 1.5 × 10^6 cells/mL in 500 μL of PBS (pH 7.4), in three replicates. Then, 0.15 MBq (25 μL, 7.0 μg, 4 μCi) of ^{89}Zr-SiR-LDFC-trastuzumab were added to 2 mL of a solution of 1% bovine serum albumin in PBS. A 50 μL aliquot of this solution was added to each microcentrifuge tube. The cell suspensions were incubated at ambient temperature for an hour. Following incubation, the tubes containing the cells were centrifuged (600 G for 2 min), and the supernatant was removed. The cell pellets were washed twice with 400 μL of cold PBS, the supernatant was removed, and the activity associated with the cell pellets were counted on the gamma counter.

Cell Imaging.

Cell Culture.—SKOV-3 cells (HER2+) were cultivated in McCoy's 5A medium (1×) supplemented with 10% fetal bovine serum and 1% penicillin/streptomycin solution under standard culture conditions. For imaging experiments, three 6-well plates were used; following the addition of 3 mL of media and coverslip, 2 × 10^4 cells in 150 μL of media were plated in each well, and the plates were incubated at 37 °C for 24 h. The media was aspirated, and the cells were washed three times with 2 mL of PBS. Then, 2 mL of PFA was added to each well, and the plate was incubated at room temperature for 1 h. Cells in one plate were treated with 4% paraformaldehyde solution (PFA) to fix cells. The PFA was aspirated, and the wells were again washed three times with cold PBS. Finally, 100 μL of SiR-LDFC-trastuzumab in serum-free media (0.1, 0.5, or 0.75 μM) was placed on a hydrophobic surface (glass plate covered with parafilm). The coverslips were removed from the wells and placed on the 100 μL immunoconjugate solution (n = 2 for each concentration). A strip of aluminum foil was folded over the plate to prevent photobleaching and evaporation of media. The glass plate was incubated at room temperature for 2 h. The coverslips were washed three times with PBS with gentle rocking and then placed into a new 6-well plate. The wells were filled with 2 mL of Hoechst staining solution in PBS (1:2000), and the coverslips were incubated for 10 min. Each coverslip was then washed again with 3 × 2 mL of PBS and mounted on a glass microplate using 30 μL of FluoroMount. Clear nail polish was used to seal the coverslip. Cells in two other plates were prepared in a similar

method but were treated with 4% PFA following the incubation with immunoconjugate solution instead ($n = 4$). No significant difference was detected between the two sample preparation methods. Confocal microscopy of the fixed cell samples was performed using a Zeiss Axio Examiner D1 modified with an Andor Differential Scanning Disk confocal unit and a 40× NA 1.0 or 20× NA 0.5 water immersion objective. SiR-LDFC-trastuzumab was imaged using the far-red filter (λ_{ex} = 618–640 nm, λ_{em} = 629–676 nm).

Imaging and Biodistribution.

All animal experiments were conducted according to the guidelines of the Institutional Animal Care and Use Committee (IACUC) at Stony Brook Medicine. Female NCr nude mice (6 weeks, Taconic Biosciences, Rensselaer, NY) were implanted subcutaneously on the right shoulder with 0.6–0.75 million SKOV-3 cells suspended in Matrigel (1:1). When the tumors reached 50–100 mm^3, the mice were anesthetized with isoflurane, and 1.1–1.9 MBq (31–52 μCi) of the immunoconjugate (37–67 μg mAb) was intravenously injected via tail vein catheter. Mice were imaged at 24, 48, 72, and 96 h post injection (p.i.) using Siemens Inveon PET/CT Multimodality System, and images were reconstructed using ASIPro software. Region of interest (ROI) analyses on all images were performed using AMIDE (Figures S5 and S6, Table S3). Fluorescence images were collected 96 h p.i. using IVIS Lumina II Imaging station equipped with Living Image software. The excitation wavelength was set to 620 nm, and emission was measured at 680 nm. Through skin, intra-surgery and post-surgery images were collected over a time period of 20 s.

Upon completion of imaging at 96 h p.i., mice were sacrificed, and select organs were harvested. Radioactivity was counted by using a gamma counter, and the radioactivity associated with each organ was expressed as %ID/g. Biodistribution data were assessed by unpaired *t*-tests using GraphPad Prism to determine if differences between groups were statistically significant ($p < 0.05$).

RESULTS

Synthesis and Characterization of Immunoconjugate.

The single-step thiourea conjugation facilitates efficient coupling of SiR-LDFC to the monoclonal antibody trastuzumab (Figure 3). Conjugation was performed by introducing NCS-functionalized SiR-LDFC to trastuzumab in a 54.5:1 molar ratio. After 18 h of incubation at ambient temperature, the immunoconjugate was isolated and purified by size exclusion chromatography. The number of incorporated fluorophores on the immunoconjugate was determined based on UV/vis spectrophotometric analysis. Taking advantage of the fluorophore absorption at 630 nm, a calibration curve was plotted for SiR-en ranging in concentration from 0.1 to 50 nmol/mL (Figure 4). Absorbance of the immunoconjugate was compared to this plot, and it corresponds to an average of 1.03 fluorophores conjugated to each antibody. This approach was validated as an adequate approximation of conjugation efficiency by direct measurement of the number of fluorophore–chelators via ESI-TOF MS/MS (Figure S2, quantification method provided in the SI). For DFO-trastuzumab, the number of chelators was quantified by ESI-TOF MS/MS,

where it was determined that each antibody was conjugated on average to two DFO chelators (Figure S3).

Fluorophore–chelator incorporation with respect to both the heavy and light chain domains was confirmed upon performing a fluorescent gel imaging analysis. Reduced and unreduced samples of SiR-LDFC-trastuzumab were resolved by SDS-PAGE, and fluorescence emission at 633 nm was visible for both heavy and light chains, as expected from nonsite-specific conjugation of the fluorophore to trastuzumab (Figure 5A,B). The DFO-trastuzumab standard was conjugated by incubating trastuzumab with 30 equiv of DFO-mesylate at ambient temperature for 18 h. Following purification, the chelator–antibody ratio was determined from ESI-TOF MS/MS (Figure S3).

Fluorescence Imaging of Cells.

Confocal microscopy techniques were employed to visualize direct binding of SiR-LDFC-trastuzumab to the cell-surface receptor HER-2 on SKOV-3 cells. SKOV-3 cells were incubated with the conjugate and counterstained with Hoechst nuclear staining dye at room temperature for 2 h before being fixed with 4% paraformaldehyde. Trastuzumab is an internalizing antibody, and this property is maintained in SiR-LDFC-trastuzumab, as evidenced by the fluorescence signal emanating from the cell surface and the cytosol (Figure 5C).

Radiolabeling, Stability, and in Vitro Properties.

DFO-trastuzumab was radiolabeled according to a previously published protocol.[23] The immunoconjugate solution was incubated with $^{89}Zr(ox)_4$ (pH = 7) at room temperature for 1 h, and the reaction progress was monitored with radio-TLC. The radiolabeled conjugate was purified, and a radiolabeling yield of 84 ± 9% (n = 3) with a specific activity of 28.5 ± 3.3 MBq/mg was obtained for ^{89}Zr-DFO-trastuzumab. Using a similar protocol, we improved radiolabeling conditions for SiR-LDFC-trastuzumab to achieve a 64 ± 9% (n = 3) radiolabeling yield with a specific activity of 30.7 ± 6.3 MBq/mg. We evaluated the in vitro immunoreactivity of ^{89}Zr-SiR-LDFC-trastuzumab using a standard Lindmo assay;[24] 53% binding was achieved (Figure S4, Table S2), which is lower than the standard ^{89}Zr-DFO-trastuzumab[25] but comparable to other modified radioimmunoconjugates reported in the literature.[26,27]

PET Imaging and Biodistribution.

We employed ^{89}Zr-SiR-LDFC-trastuzumab for in vivo evaluation of the HER2-overexpressing tumor burden using nuclear and fluorescent imaging modalities in a conventional mouse tumor xenograft model. The performance was directly compared to ^{89}Zr-DFO-trastuzumab with respect to PET imaging performance (ROI) and biodistribution. 1.1–1.3 MBq (31–35 μCi, 37–42 μg) of ^{89}Zr-SiR-LDFC-trastuzumab and 1.4–1.9 MBq (37–52 μCi, 47–67 μg) of ^{89}Zr-DFO-trastuzumab were administered to the mice via tail vein catheter. Subsequently, mice were imaged via PET/CT at 24, 48, 72, and 96 h p.i. For both conjugates, tumor uptake was visible at 24 h p.i. and gradually increased over time, as quantified by ROI analysis (Figures 6A,B, S5, and S7). The uptake of ^{89}Zr-SiR-LDFC-trastuzumab within the tumor was not significantly different from that of ^{89}Zr-DFO-

trastuzumab, indicating that the presence of fluorophore does not adversely affect the targeting affinity of trastuzumab. Additionally, the biodistribution of ^{89}Zr-SiR-LDFC-trastuzumab was not statistically different from that of ^{89}Zr-DFO-trastuzumab (Figure 7). These results are mostly consistent with the biodistribution of the immunoconjugates in naive C57BL6 mice.[23] Prior investigation of ^{89}Zr-LDFC-trastuzumab conjugates in naïve mice found an increased bone and decreased liver uptake when compared to ^{89}Zr-DFO-trastuzumab. These results correlate well with data obtained in this study; while not statistically significant, the average uptake is higher in the bone and lower in liver for ^{89}Zr-SiR-LDFC-trastuzumab (Table 1).

Fluorescence imaging was performed at 96 h p.i. to determine the potential of the conjugate as an intrasurgical guide during the resection of a tumor mass. In vivo imaging showed high fluorescence at the site of tumor (Figure 8A, left). Areas on the face and back are fluorescent due to contamination issues involving the imaging probe by coprophagy and subsequent grooming.[28] Initially, animals were imaged without any modification (Figure S8A). However, the stomach is an area of high intrinsic fluorescence, as exemplified by the control image: A healthy nude mouse with no fluorophore injection shows intense fluorescence in the abdominal area (Figure S8B) under identical fluorescence imaging settings employed.

We proceeded to emulate a surgical setting. The skin tissue covering the tumor was removed following identification of the primary tumor mass via noninvasive, through skin imaging (Figure 8A, left). A clear separation of the tumor from its surrounding tissue was visible (Figure 8A, middle). Upon successful excision of the tumor, no fluorescence was detected in the surrounding tissue; whereas, the resected tumor remains fluorescent (Figure 8A, right). The fluorescence of the tumor and pertinent organs were imaged ex vivo, and fluorescence was only visible in the tumor (Figure 8B), underscoring results obtained by PET imaging that indicated a favorable off-target clearance profile of the SiR-LDFC-conjugate.

DISCUSSION

Varying the number of fluorophores attached to an antibody can significantly alter the pharmacokinetics of the immunoconjugate. Therefore, conjugation conditions need to be carefully adjusted to achieve a reproducible antibody–fluorophore ratio.[1,20,29] When constructing multimodal imaging probes, a single-step conjugation of fluorophore and chelator to the targeting unit is desirable in order to minimize heterogeneity in the resulting immunoconjugates. By conjugating the fluorophore and chelator to the antibody simultaneously as a single unit, complex procedures for controlling the fluorophore–chelator ratio can be circumvented. SiR-LDFC-trastuzumab can be prepared in a true one-step reaction, and the resulting immunoconjugate is functionalized with a fluorophore and a chelator in a 1:1 ratio via coupling to a lysine residue intrinsic to the antibody. Upon conjugation, UV–vis absorbance of the attached fluorophore can be utilized to determine the antibody–conjugate ratio in the absence of Q-TOF MS/MS instrumentation.

In addition to providing a convenient method for conjugate characterization, SiR-LDFC-trastuzumab also displays improved performance in the biodistribution and in vivo imaging applications compared to DFO-BODIPY-trastuzumab.[14] The high lipophilicity of BODIPY

was found to alter the pharmacokinetics of the targeting antibody, resulting in increased uptake of DFO-BODIPY-trastuzumab in liver and tumor when compared to the standard DFO-trastuzumab. Presence of SiR-LDFC, on the other hand, does not have a significant impact on the targeting affinity or off-target uptake of trastuzumab. The biodistributions of SiR-LDFC-trastuzumab and DFO-trastuzumab were found to be statistically equivalent. Our prior work indicated accelerated blood clearance of LDFC immunoconjugates, which can lead to decreased probe uptake at the target. However, the targeted imaging experiments in this article have confirmed this to not be an issue. The observed trends of a slight elevation in bone uptake prevail, possibly suggesting a lower stability of ^{89}Zr-SiR-LDFC-trastuzumab than ^{89}Zr-DFO-trastuzumab, but the differences were not found to be statistically significant. We note that the uptake of ^{89}Zr-DFO-trastuzumab in liver is slightly higher in this study than literature values,[25,30] but it is not statistically significant due to the large error. Finally, SiR emits fluorescence at longer wavelengths (633 nm) than BODIPY (488 nm), enabling in vivo through-skin and ex vivo optical imaging of tumors in mice, demonstrating the utility and clinical potential of this probe. Future work will include variation of the fluorophore structure with emission properties within the NIR region, as well as incorporation of drug molecules onto the LDFC scaffold for direct radiolabeling of antibody–drug conjugates. The chemical versatility of LDFC provides a convenient, in vivo applicable handle for the ^{89}Zr-radiolabeling of a wide array of antibody conjugates. Studies to expand on the multimodality applications presented here are ongoing.

CONCLUSIONS

We conjugated a radioisotope chelator–fluorophore conjugate to the HER2 targeting antibody trastuzumab in one step and successfully radiolabeled the immunoconjugate with ^{89}Zr. The single-step conjugation is advantageous over previously reported two-step conjugation because it provides direct control of the antibody-to-radioisotope-to-fluorophore ratio and results in reduced heterogeneity of the construct.[14] The presence of fluorophore does not alter the targeting affinity of trastuzumab, while ^{89}Zr-SiR-LDFC-trastuzumab was found to behave similarly to the standard DFO conjugate in vivo. Imaging with PET/CT and fluorescence modalities takes advantage of the high accumulation of SiR-LDFC-trastuzumab in the tumor mass. Following whole-body PET imaging studies, we performed a fluorescence-guided excision of the tumor xenograft to demonstrate the applicability of optical imaging as an intrasurgical diagnostic tool. The short-wavelength emission of SiR may be inadequate for imaging tumors deeply nested in vivo but may be more suitable as a topical imaging probe. However, LDFC offers a modular platform for conjugation of any fluorophore through peptide linkage, and the trifunctional nature of LDFC enables conjugation to other targeting vectors, such as peptides and/or small molecules. Subsequent work on the conjugation of near-IR emitting dyes and drug payloads to small molecules and antibodies via LDFC is underway.

Supplementary Material

Refer to Web version on PubMed Central for supplementary material.

ACKNOWLEDGMENTS

E.B. acknowledges funding sources, specifically the NIH for a Pathway to Independence Award (NHLBI R00HL125728-03), a REACH award (U01HL127522-18150031), and Stony Brook University for startup funds.

REFERENCES

(1). Sampath L; Kwon S; Ke S; Wang W; Schiff R; Mawad ME; Sevick-Muraca EM Dual-labeled trastuzumab-based imaging agent for the detection of human epidermal growth factor receptor 2 overexpression in breast cancer. J. Nucl. Med 2007, 48, 1501–1510. [PubMed: 17785729]

(2). Maindron N; Ipuy M; Bernhard C; Lhenry D; Moreau M; Carme S; Oudot A; Collin B; Vrigneaud JM; Provent P; Brunotte F; Denat F; Goze C Near infrared emitting BODIPY trisDOTA^{111}In as a monomolecular multifunctional imaging probe: from synthesis to in vivo investigations. Chem. - Eur. J 2016, 22, 12670–12674. [PubMed: 27410465]

(3). Lewis Phillips GD; Li G; Dugger DL; Crocker LM; Parsons KL; Mai E; Blattler WA; Lambert JM; Chari RVJ; Lutz RJ; Wong WLT; Jacobson FS; Koeppen H; Schwall RH; Kenkare-Mitra SR; Spencer SD; Sliwkowski MX Targeting HER2-positive breast cancer with trastuzumab-DM1, an antibody–cytotoxic drug conjugate. Cancer Res 2008, 68, 9280–9290. [PubMed: 19010901]

(4). Verma S; Miles D; Gianni L; Krop IE; Welslau M; Baselga J; Pegram M; Oh D-Y; Diéras V; Guardino E; Fang L; Lu MW; Olsen S; Blackwell K Trastuzumab emtansine for HER2-positive advanced breast cancer. N. Engl. J. Med 2012, 367, 1783–1791. [PubMed: 23020162]

(5). LoRusso PM; Weiss D; Guardino E; Girish S; Sliwkowski MX Trastuzumab emtansine: A unique antibody-drug conjugate in development for human epidermal growth factor receptor 2–positive cancer. Clin. Cancer Res 2011, 17, 6437–6447. [PubMed: 22003071]

(6). Schibli R; Schubiger AP Current use and future potential of organometallic radiopharmaceuticals. Eur. J. Nucl. Med. Mol. Imaging 2002, 29, 1529–1542. [PubMed: 12397472]

(7). Buck A; Schirrmeister H; Kühn T; Shen C; Kalker T; Kotzerke J; Dankerl A; Glatting G; Reske S; Mattfeldt T FDG uptake in breast cancer: correlation with biological and clinical prognostic parameters. Eur. J. Nucl. Med. Mol. Imaging 2002, 29, 1317–1323. [PubMed: 12271413]

(8). Ben-Haim S; Ell P 18F-FDG PET and PET/CT in the evaluation of cancer treatment response. J. Nucl. Med 2008, 50, 88–99.

(9). Alavi A; Werner TJ FDG-PET imaging to detect and characterize infectious disorders; an unavoidable path for the foreseeable future. Eur. J. Nucl. Med. Mol. Imaging 2017, 44, 417–420. [PubMed: 28039496]

(10). Alavi A; Kung JW; Zhuang H Implications of PET based molecular imaging on the current and future practice of medicine. Semin. Nucl. Med 2004, 34, 56–69. [PubMed: 14735459]

(11). Vansteenkiste JF; Stroobants SG; Dupont PJ; De Leyn PR; De Wever WF; Verbeken EK; Nuyts JL; Maes FP; Bogaert JG FDG-PET scan in potentially operable non-small cell lung cancer: do anatometabolic PET-CT fusion images improve the localisation of regional lymph node metastases? Eur. J. Nucl. Med. Mol. Imaging 1998, 25, 1495–1501.

(12). Pandey SK; Gryshuk AL; Sajjad M; Zheng X; Chen Y; Abouzeid MM; Morgan J; Charamisinau I; Nabi HA; Oseroff A; Pandey RK Multimodality agents for tumor imaging (PET, fluorescence) and photodynamic therapy. A possible “see and treat” approach. J. Med. Chem 2005, 48, 6286–6295. [PubMed: 16190755]

(13). Hendricks JA; Keliher EJ; Wan D; Hilderbrand SA; Weissleder R; Mazitschek R Synthesis of [^{18}F] BODIPY: bifunctional reporter for hybrid optical/positron emission tomography imaging. Angew. Chem 2012, 124, 4681–4684.

(14). Meimetis LG; Boros E; Carlson JC; Ran C; Caravan P; Weissleder R Bioorthogonal fluorophore linked DFO- technology enabling facile chelator quantification and multimodal imaging of antibodies. Bioconjugate Chem 2016, 27, 257–263.

(15). Schubiger P; Grünberg J; Ametamey SM; Honer M; Garcia-Garayoa E; Blauenstein P; Waibel R; Novak-Hofer I; Schibli R Radiopharmaceuticals: from molecular imaging to targeted radionuclide therapy. Chimia 2004, 58, 731–735.

(16). Predina JD; Newton AD; Xia L; Corbett C; Connolly C; Shin M; Sulyok LF; Litzky L; Deshpande C; Nie S; et al. An open label trial of folate receptor-targeted intraoperative molecular imaging to localize pulmonary squamous cell carcinomas. Oncotarget 2018, 9, 13517. [PubMed: 29568374]

(17). Rosenthal EL; Warram JM; de Boer E; Chung TK; Korb ML; Brandwein-Gensler M; Strong TV; Schmalbach CE; Morlandt AB; Agarwal G; et al. Safety and tumor specificity of cetuximab-IRDye800 for surgical navigation in head and neck cancer. Clin. Cancer Res 2015, 21, 3658–3666. [PubMed: 25904751]

(18). Rieffel J; Chitgupi U; Lovell JF Recent advances in higher-order, multimodal, biomedical imaging agents. Small 2015, 11, 4445–4461. [PubMed: 26185099]

(19). Xing Y; Zhao J; Conti PS; Chen K Radiolabeled nanoparticles for multimodality tumor imaging. Theranostics 2014, 4, 290–306. [PubMed: 24505237]

(20). Rijpkema M; Bos DL; Cornelissen AS; Franssen GM; Goldenberg DM; Oyen WJ; Boerman OC Optimization of dual-labeled antibodies for targeted intraoperative imaging of tumors. Mol. Imaging 2015, 14, 348–355. [PubMed: 26162516]

(21). Guo Y; Yuan H; Rice WL; Kumar ATN; Goergen CJ; Jokivarsi K; Josephson L The PEG-fluorochrome shielding approach for targeted probe design. J. Am. Chem. Soc 2012, 134, 19338–19341. [PubMed: 23137147]

(22). Loudet A; Burgess K BODIPY Dyes and their derivatives: syntheses and spectroscopic properties. Chem. Rev 2007, 107, 4891–4932. [PubMed: 17924696]

(23). Adams CJ; Wilson JJ; Boros E Multifunctional Desferrichrome Analogues as Versatile ^{89}Zr(IV) Chelators for ImmunoPET Probe Development. Mol. Pharmaceutics 2017, 14, 2831–2842.

(24). Lindmo T; Boven E; Cuttitta F; Fedorko J; Bunn PA Determination of the immunoreactive function of radiolabeled monoclonal antibodies by linear extrapolation to binding at infinite antigen excess. J. Immunol. Methods 1984, 72, 77–89. [PubMed: 6086763]

(25). Holland JP; Caldas-Lopes E; Divilov V; Longo VA; Taldone T; Zatorska D; Chiosis G; Lewis JS Measuring the pharmacodynamic effects of a novel Hsp90 inhibitor on HER2/neu expression in mice using ^{89}Zr-DFO-trastuzumab. PLoS One 2010, 5, e8859. [PubMed: 20111600]

(26). Moreau M; Raguin O; Vrigneaud J-M; Collin B; Bernhard C; Tizon X; Boschetti F. d. r.; Duchamp O; Brunotte F. o.; Denat F DOTAGA-trastuzumab. A new antibody conjugate targeting HER2/Neu antigen for diagnostic purposes. Bioconjugate Chem 2012, 23, 1181–1188.

(27). McLarty K; Cornelissen B; Scollard DA; Done SJ; Chun K; Reilly RM Associations between the uptake of ^{111}In-DTPA-trastuzumab, HER2 density and response to trastuzumab (Herceptin) in athymic mice bearing subcutaneous human tumour xenografts. Eur.J. Nucl. Med. Mol. Imaging 2009, 36, 81–93. [PubMed: 18712381]

(28). Kenagy G; Hoyt DF Reingestion of feces in rodents and its daily rhythmicity. Oecologia 1979, 44, 403–409. [PubMed: 28310297]

(29). Zeglis BM; Davis CB; Abdel-Atti D; Carlin SD; Chen A; Aggeler R; Agnew BJ; Lewis JS Chemoenzymatic strategy for the synthesis of site-specifically labeled immunoconjugates for multimodal PET and optical imaging. Bioconjugate Chem 2014, 25, 2123–2128.

(30). Heskamp S; Raavé R; Boerman O; Rijpkema M; Goncalves V; Denat F ^{89}Zr-immuno-positron emission tomography in oncology: state-of-the-art ^{89}Zr radiochemistry. Bioconjugate Chem 2017, 28, 2211–2223.

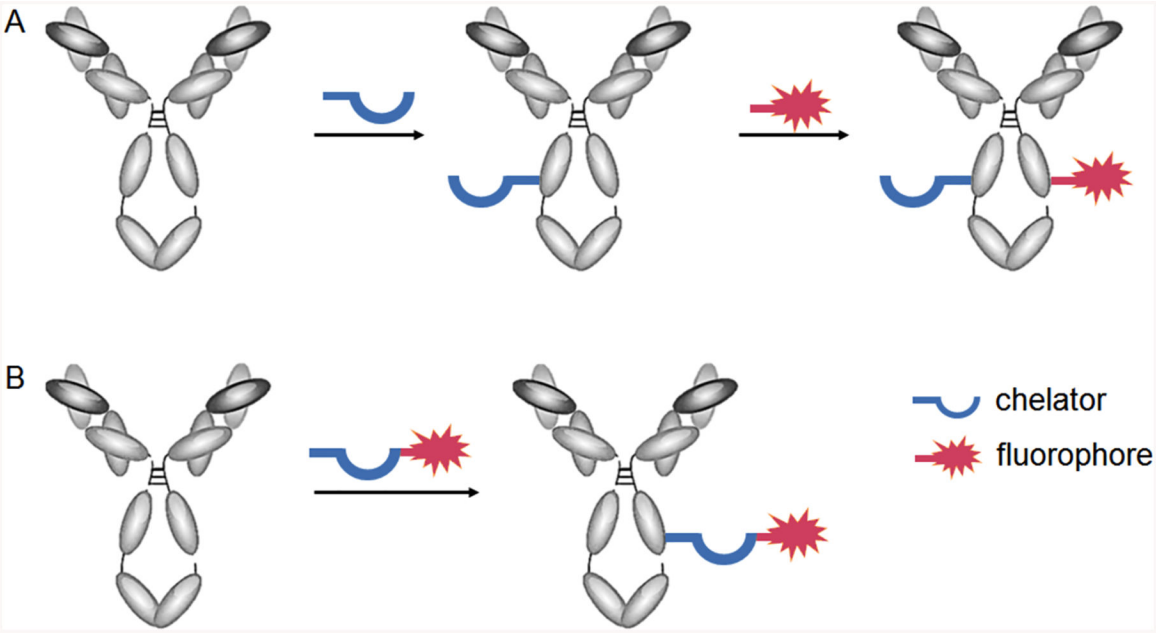

Figure 1.
Stepwise (A) and concerted (B) conjugation of radiometal chelator and fluorophore to antibody.

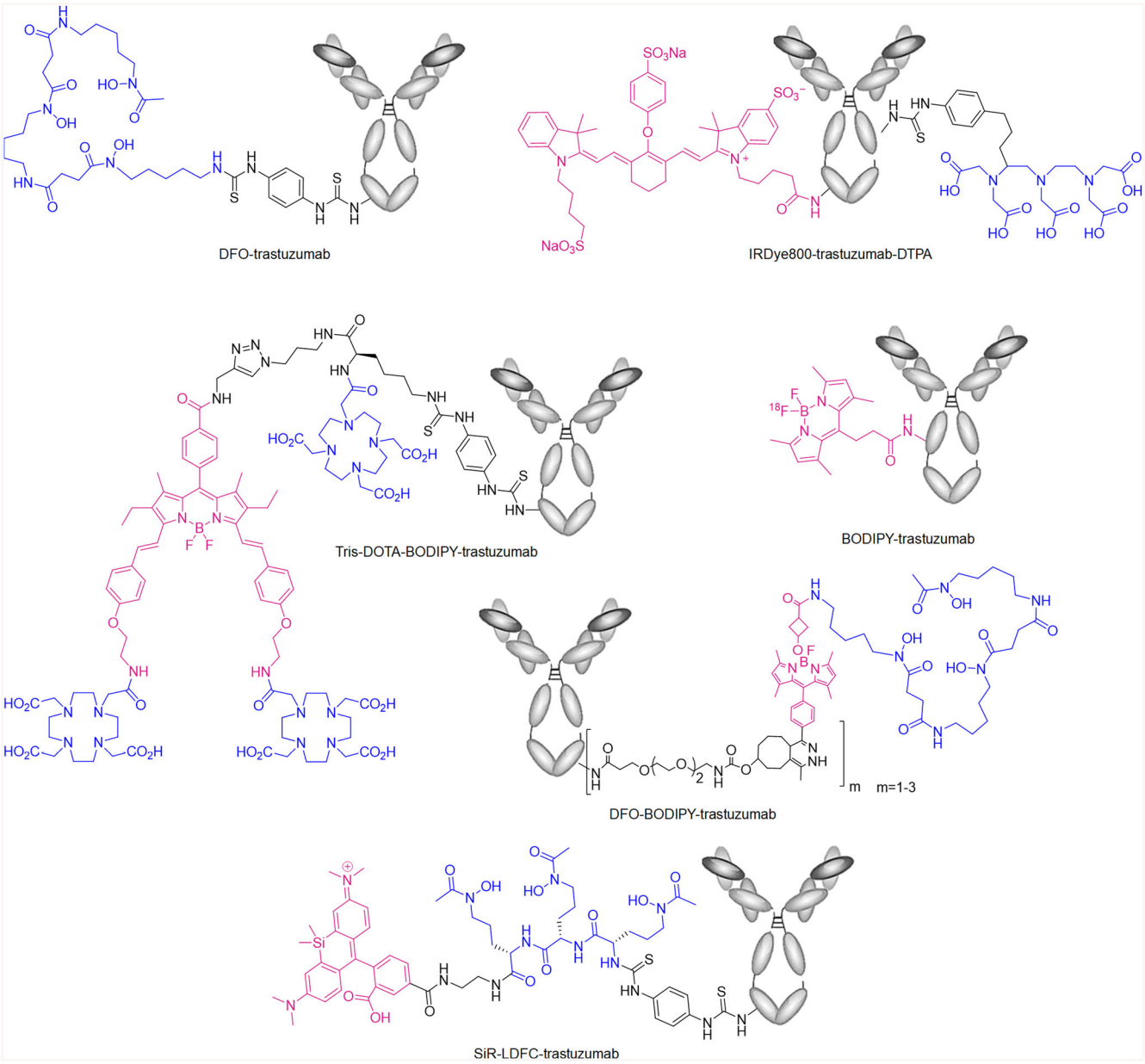

Figure 2.

Structure of DFO-trastuzumab and literature-reported bimodal imaging probes IRDye800-trastuzumab-DTPA,[1] tris-DOTA-BODIPY-trastuzumab,[2] BODIPY-trastuzumab,[13] DFO-BODIPY trastuzumab,[14] and SiR-LDFC-trastuzumab (this work). Fluorophores are indicated in magenta, radiometal chelators in blue.

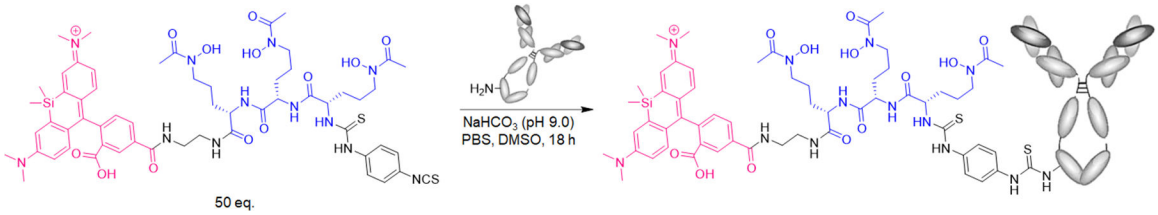

Figure 3.
Synthetic scheme for SiR-LDFC-trastuzumab.

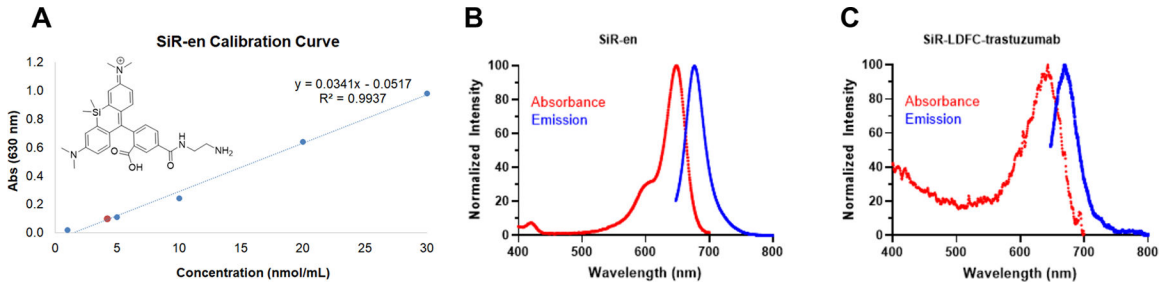

Figure 4.

(A) Calibration curve of the absorbance of SiR-en at 630 nm; red marker indicates absorbance of SiR-LDFC-trastuzumab. Absorbance and emission spectra of (B) SiR-en and (C) SiR-LDFC-trastuzumab at a protein concentration of 4 nmol/mL (λ_{Ex} = 630 nm).

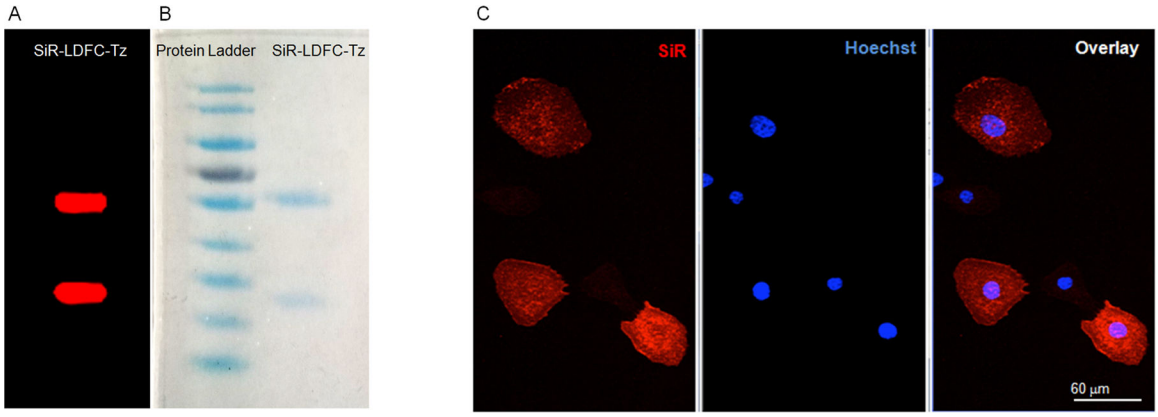

Figure 5.

Gel electrophoresis of SiR-LDFC-trastuzumab visualized by (A) fluorescence imaging at 633 nm and (B) Coomassie staining. (C) Confocal microscopy images of SKOV-3 cells treated with SiR-LDFC-trastuzumab (red, SiR; blue, Hoechst 33342). Scale bar represents 60 μm.

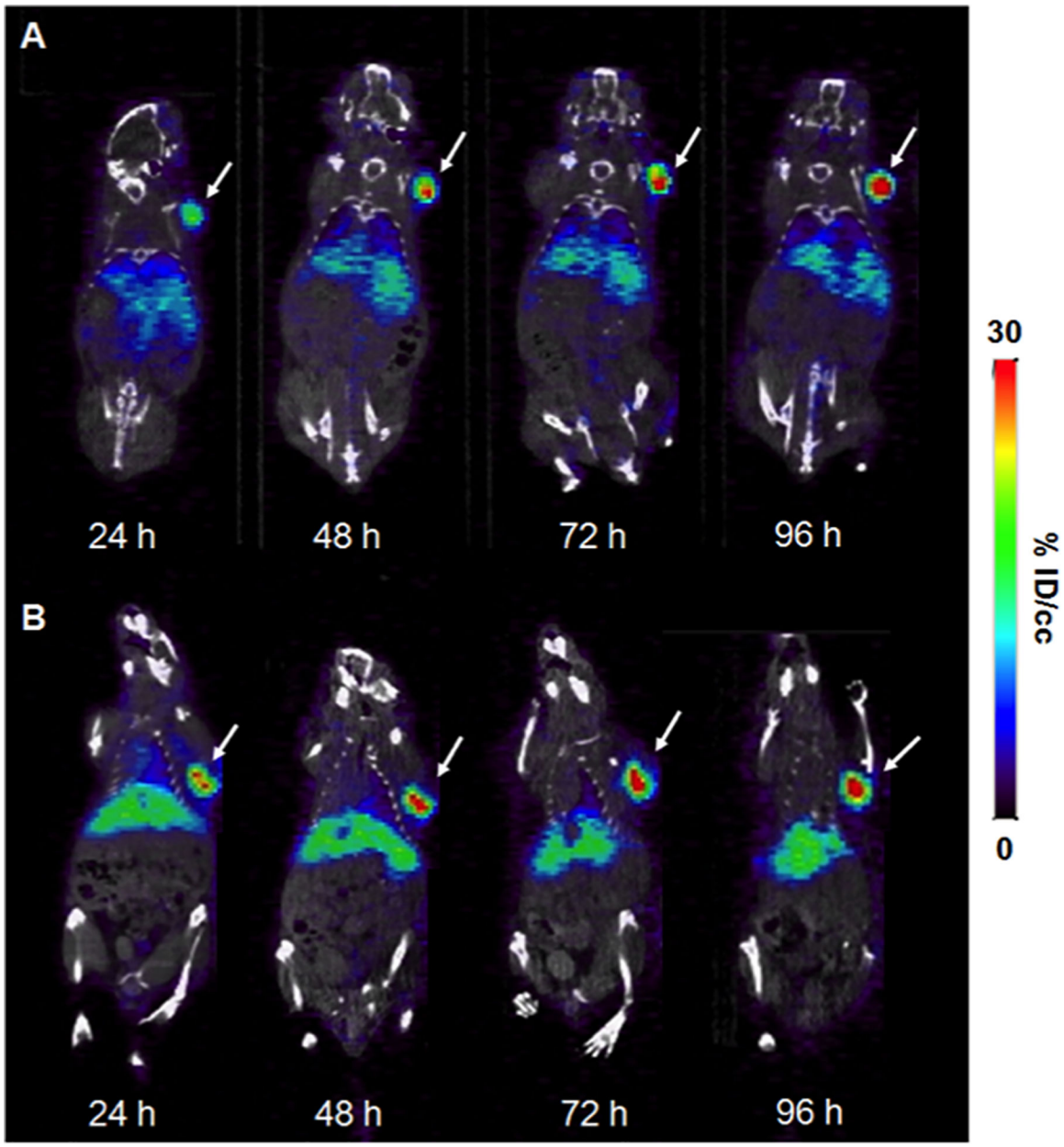

Figure 6.

Single slice coronal ^{89}Zr-SiR-LDFC-trastuzumab (A) and ^{89}Zr-DFO-trastuzumab (B) PET/CT images in SKOV-3 subcutaneous tumor-bearing mice ($n = 4$) at 24, 28, 72, and 96 h p.i. Tumor indicated by white arrow.

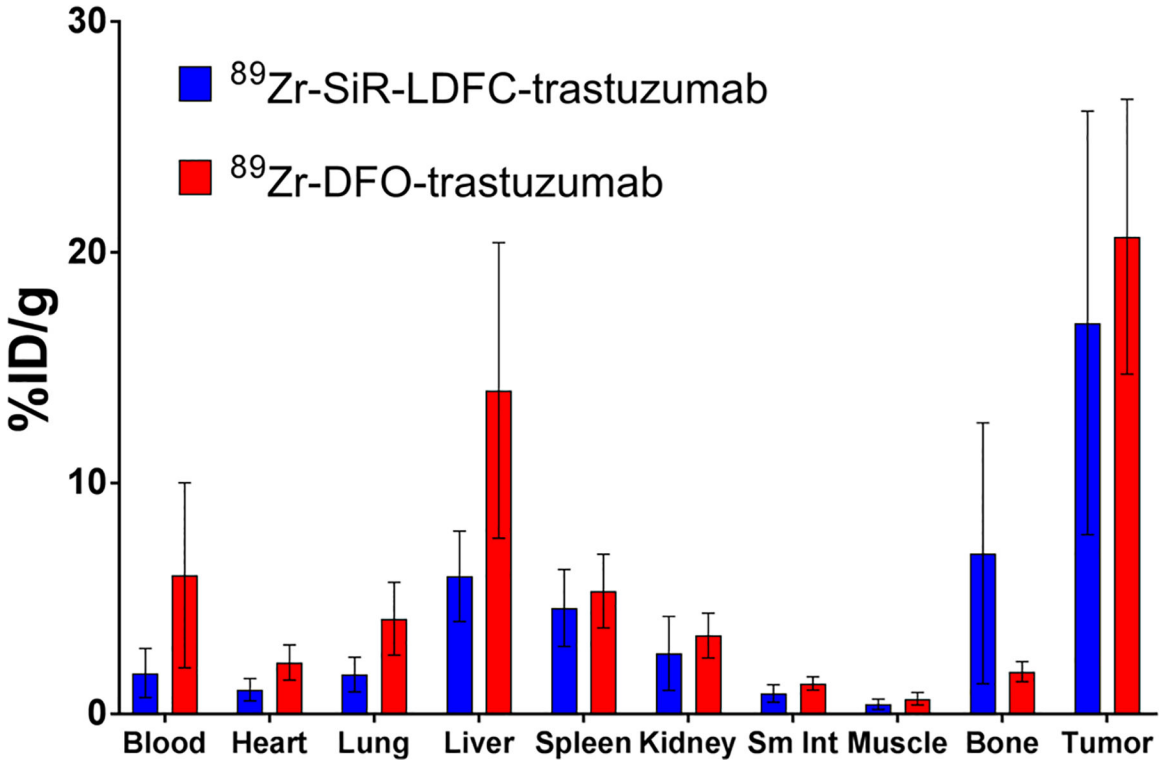

Figure 7.
Biodistribution of ^{89}Zr-SiR-LDFC-trastuzumab and ^{89}Zr-DFO-trastuzumab in SKOV-3 subcutaneous xenografts (n = 4) at 96 h p.i.

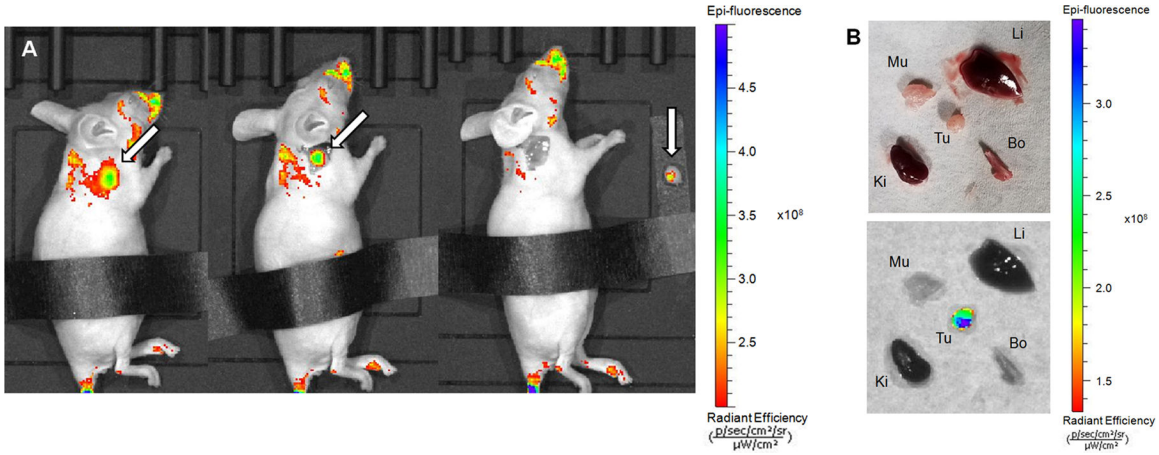

Figure 8.

(A) Fluorescence image of SKOV-3 tumor-bearing mouse injected with ^{89}Zr-SiR-LDFC-trastuzumab at 96 h p.i., before tumor resection (left), with skin removed (middle), and after tumor resection (right). Tumor indicated by white arrow. (B) Ex vivo imaging of organs collected from SKOV-3 tumor-bearing mouse injected with ^{89}Zr-SiR-LDFC-trastuzumab at 96 h p.i. under white light (top) and excited at 620 nm (bottom). The abdominal area was covered to minimize autofluorescence effects.

Table 1.

Biodistribution of ^{89}Zr-SiR-LDFC-trastuzumab (n = 4) and ^{89}Zr-DFO-trastuzumab (n = 5) at 96 h p.i. in Nude Mice Bearing SKOV-3 Xenografts

	biodistribution 96 h p.i. (% ID/g ± stdev)	
	^{89}Zr-SiR-LDFC-trastuzumab	**^{89}Zr-DFO-trastuzumab**
blood	1.77 ± 1.06	6.01 ± 4.01
heart	1.05 ± 0.48	2.23 ± 0.77
lung	1.71 ± 0.75	4.12 ± 1.58
liver	5.96 ± 1.96	14.0 ± 6.4
spleen	4.60 ± 1.67	5.33 ± 1.60
kidney	2.62 ± 1.60	3.40 ± 0.97
small intestine	0.89 ± 0.38	1.32 ± 0.29
muscle	0.41 ± 0.23	0.66 ± 0.27
bone	6.96 ± 5.65	1.83 ± 0.44
tumor	16.9 ± 9.2	20.7 ± 6.0